Front. Phys. 13(5), 138116 (2018)
https://doi.org/10.1007/s11467-018-0808-9

RESEARCH ARTICLE

Molecular-scale processes affecting growth rates of ice at moderate supercooling

Rui Wang[1], **Li-Mei Xu**[1,†], **Feng Wang**[2,‡]

[1] *International Center for Quantum Materials and School of Physics, Peking University, No. 5 Yiheyuan Road, Beijing 100871, China*
[2] *Department of Chemistry and Biochemistry, University of Arkansas, Fayetteville, AR 72701, USA*
Corresponding authors. E-mail: [†] *limei.xu@pku.edu.cn,* [‡] *fengwang@uark.edu*
Received May 15, 2018; accepted June 2, 2018

The growth kinetics of ice are modeled using the Water Potential from Adaptive Force Matching for Ice and Liquid (WAIL) potential with molecular dynamics. The all-atom WAIL model provides a good description of the properties of both ice and liquid with an equilibrium temperature of 270 K at 1 bar. The growth kinetics captured by this model can thus reflect those of real ice. Our simulation indicates that the growth rate of ice on the basal plane is fastest at approximately 20 K supercooling, consistent with experimental findings, where the growth rate increases monotonically as the supercooling increases to 18 K. The key factors that control the growth kinetics leading to the optimal growth temperature are investigated. The simulation revealed a bilayer-by-bilayer growth mechanism on the basal plane that proceeds in two steps. Whereas water molecules lose translational motion and become ice-like quickly, the establishment of orientational order to form ice is a slow and activated process. Enhanced by the templating effect of sublayers, the rapid reduction in translational motion in the formation of the prefreezing layer might explain the significantly faster growth rate relative to the nucleation rate of water. Whereas remelting of the prefreezing layer is observed at low supercooling and may be responsible for the lower growth rate close to the melting temperature, the slow orientational ordering of the prefreezing layer into the final ice conformation is partly responsible for the reduced growth rate at deeper supercooling.

Keywords ice growth, interface water, dynamics of crystallization

PACS numbers 81.10.-h, 68.08.-p, 02.70.Ns

1 Introduction

Water has many intriguing behaviors that have not been clearly explained. The anomalous properties of deeply supercooled water attract much research attention [1–4]. The study of water on surfaces plays an important role in biology [5–9]. In particular, the hydrogen bond interactions in water systems directly influence many physiochemical processes [10–13]. Moreover, the crystallization of water on surfaces is an essential process in various technologies. Liquid water can be supercooled easily. Once ice nucleates, either by homogenous or heterogeneous means, the growth of ice is relatively fast. The growth rates of ice on surfaces influence the difficulty of deicing of mission critical structures, such as airplane wings or fuselages. A better understanding of ice growth on surfaces is important for innovative strategies for the promotion or prevention of icing [14–19]. The study of ice nucleation and growth has received significant attention, both experimentally [20–22] and theoretically [23–25]. The experimental measurements of nucleation and growth rates generally do not directly reveal the atomistic details of the growth kinetics. The growth rate of ice increases initially as supercooling increases below the freezing temperature. Whereas it is anticipated that growth should slow down below the temperature of maximum rate as a result of slower diffusion, existing experiments show a monotonic increase in growth rate up to 18 K of supercooling [26–28]. The growth rate measured with molecular dynamics generally suggests the maximum growth rates occur at approximately 10 K of supercooling [25, 29]. The disagreement between theory and experiments is not surprising, considering that var-

Frontiers of Physics

ious approximations made in simulations. For example, most simulations use a thermostat that involves rescaling of atomic velocities, and thus the procedure is not able to capture the true influence of heat dissipation on growth rates [30, 31]. In addition, it is anticipated that the temperature of maximum growth rate in a simulation is strongly influenced by the model potential used for water.

In this work, we study the growth kinetics of ice with the Water potential from Adaptive force matching for Ice and Liquid (WAIL) model [32]. WAIL is one of the few models that reproduce the true T_M of water within 5 K. We note that the WAIL potential was developed by only fitting to high-accuracy electronic structure gradients, and thus the 270 K T_M of WAIL is not simply a result of fitting to experiments. It might provide the least biased description of the growth kinetics of water at the atomistic scale. Whereas a brute-force simulation of nucleation has been done with the coarse-grained mW potential [33], an all-atomistic description would require enhanced sampling methods, such as seeding [34, 35] and forward flux sampling [36]. Evidences have shown different kinetics produced by a a result of the enhanced sampling algorithms. In this work, we focus on a brute-force simulation of the growth kinetics on the basal plane of ice. The focus is to establish the temperature of maximum growth rate. Attention will be paid to the growth mechanisms and the microscopic processes that influence the growth rate at different degrees of supercooling. With an all-atom potential, one limitation would be the fairly small system used to allow sufficient simulation length to provide more reliable statistics. The finite size limitation should be kept in mind when the simulation results are used to interpret real world phenomena.

The paper is composed of four sections. After the introduction, the simulation details, such as the choice of order parameters and identification of different layers of growth, are discussed in Section 2. The results and discussions are presented in Section 3, with the main conclusion summarized in Section 4.

2 Simulation details

2.1 Simulation protocol

The system contains an ice box with 300 water molecules and a slab of liquid water with 1500 molecules on top of the ice. In order to avoid possible complications with barostats, we perform NVT simulations in the system with a vacuum region of 3.5 nm wide above the liquid, as shown in Fig. 1. Periodic boundary conditions are applied in the x, y, and z directions.

Both ice Ih and ice Ic are proton-disordered. Because

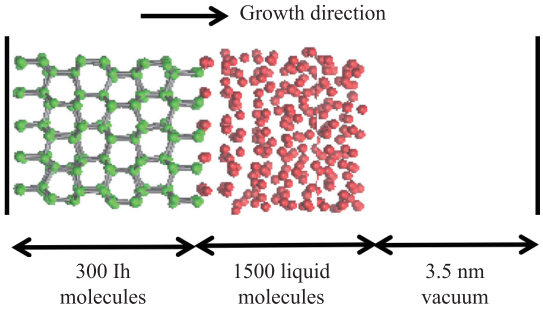

Fig. 1 Illustration of an initial configuration. The system contains six fixed layers of 300 hexagonal ice (Ih) molecules (green) with the basal face (perpendicular to z) exposed to 1500 liquid water molecules (red), and vacuum above the liquid.

the inter-conversion between different proton arrangements is slow, choosing any one initial proton arrangement could lead to biased sampling. In this work, a total of 20 ice Ih conformations with 300 water molecules were generated with the electrostatic switching method [37] to sample independent proton arrangements of ice. Each ice box was equilibrated under the NPT ensemble for 2 ns to obtain the initial lattice vectors, which depend weakly on the proton arrangement. In the x–y dimensions, such a procedure leads to approximate lengths of 2.28 and 1.98 nm for the a and b lattice vectors, respectively, at an angle of 60°. The slab was constructed by extending the c lattice vector orthogonally to the x–y plane, to a length of 16.0 nm. The 300 ice Ih molecules formed six bilayers of ice, which are fixed to their bulk positions. An additional 1500 liquid molecules were introduced on top of the ice molecules for the study of ice growth. The choice of 16.0 nm for the c lattice vector allows approximately 3.5 nm of vacuum on top of the liquid in the initial conformation before the additional ice formation.

All the simulations were performed using the GROMACS simulation package [38]. The coulombic interactions were treated with a 4th-order particle mesh Ewald method with 0.1 nm spacing for the reciprocal Ewald sum. The real-space cutoff for the coulombic interaction was 0.9 nm, which was also the cutoff for the van der Waals interactions. From each initial configuration, NVT simulations is performed at five different temperatures from 240 to 260 K with a timestep of 0.5 fs. The system temperature was controlled with the Nosé Hoover thermostat with a relaxation constant of 2.0 ps. Each trajectory was simulated until the potential energy levelled off, suggesting the end of growth. This leads to trajectories lasting 100 to 160 ns, depending on the conformation and temperature. The coordinates of molecules are recorded every 10 ps for our analysis.

2.2 Identification of different forms of ice and water

Part of the complication of the growth kinetics arises from the complex phase diagram of ice. Although the only thermodynamically stable phase at ambient pressure slightly below 0 °C is ice Ih, the metastable ice Ic has been observed during freezing, both in experiments [39, 40] and simulations [41, 42].

Ice Ih and ice Ic are very similar, both structurally and thermodynamically. Each water molecule forms four hydrogen bonds and satisfies the so-called ice rules in both phases [43]. The basal (0001) plane of ice Ih and the (111) plane of ice Ic are identical, with each water participating in three different six-membered rings while forming one hydrogen bond with an adjacent layer. As shown in Fig. 2, both ice Ih and ice Ic can be seen as a stack of a series of bilayers. Whereas all the bilayers in ice Ic are identical, every other bilayer in the ice Ih structure is flipped. Consequently, it is difficult to distinguish between ice Ih and ice Ic from one bilayer; the two forms of ice can only be distinguished by observing the relative orientation of two bilayers. Owing to the close similarity of the two phases of ice, it is not surprising that ice Ic grows spontaneously on ice Ih and vice versa, leading to stacking disorder [42].

In our simulation, both ice Ih and Ic grow competitively, leading to stacking disorder. In order to properly monitor the growth kinetics, it is important to reliably distinguish liquid, ice Ih, and ice Ic. Various order parameters have been designed to distinguish the three forms of water [44–48].

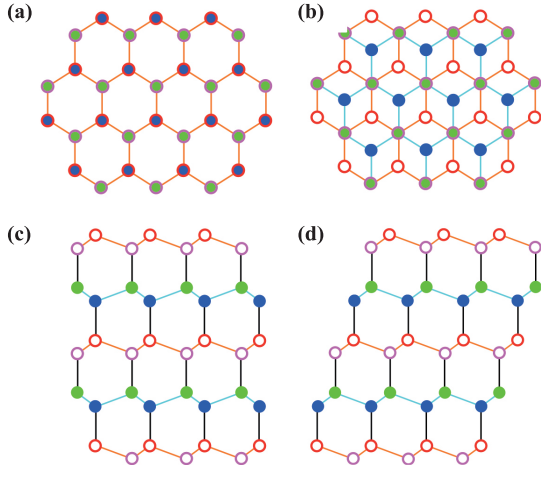

Fig. 2 The structure of ice Ih and ice Ic. Comparison of the top views of ice Ih **(a)** and ice Ic **(b)** crystal structures, in an overlay of two bilayers. The red oxygens are located above the plane of the figure. The magenta oxygens are located below the plane of the figure. In both structures, the blue oxygens are not hydrogen bonded to any of the waters in the red-magenta bilayer shown. The magenta and green oxygens are hydrogen bonded. Comparison of the side views of ice Ih **(c)** and ice Ic **(d)**. Bilayers stack in an ABAB pattern in ice Ih while stack in an ABCABC pattern in ice Ic.

For distinguishing between ice Ih and ice Ic, one of the most effective parameters is the correlation between the orientational bond order of water molecules i and j [46, 47], $c(i,j)$. This can be conveniently determined using the q_{lm} order parameter, defined as

$$q_{lm} = \frac{1}{N_n(i)} \sum_{j=1}^{N_n(i)} Y_{lm}(\theta_{ij}, \varphi_{ij}) \ , \tag{1}$$

where $N_n(i)$ is the number of neighbors of particle i and $Y_{lm}(\theta_{ij}, \varphi_{ij})$ are standard Laplace spherical Harmonics, which are complex. θ_{ij} and φ_{ij} are the polar and azimuthal angles of the vector from the oxygen atom of water i to that of water j. In this work, a water molecule is considered as a neighbor of another molecule if their oxygen–oxygen distance is less than 0.35 nm. With an l value of 3, the orientational bond order is defined as

$$\begin{aligned} c(i,j) &= \frac{q_3(i) \cdot q_3(j)}{|q_3(i)||q_3(j)|} \\ &= \frac{\sum_{m=-3}^{3} q^*_{3m}(i) q^*_{3m}(j)}{\left(\sum_{m=-3}^{3} q^*_{3m}(i) q^*_{3m}(i)\right)\left(\sum_{m=-3}^{3} q^*_{3m}(j) q^*_{3m}(j)\right)} . \end{aligned} \tag{2}$$

For each ice molecule i, j is one of its four nearest neighbor molecules. For ice Ic, all four $c(i,j)$ of each water are in the range from -0.75 to -1.0. For ice Ih, one of the four $c(i,j)$ is in the range from -0.3 to 0.25, and the other three are in the same range as that for ice Ic [Fig. 3(b)].

Although $c(i,j)$ shows a clear difference between ice Ih and ice Ic, many molecules in liquid water could be transiently identified as ice if it were to be used as the only order parameter. In order to achieve better distinction between ice and liquid [48], we also leveraged the neighbor-averaged q_6 parameter,

$$q_{n6}(i) = \left(\frac{4\pi}{13} \sum_{m=-6}^{6} |\langle q_{6m}(i) \rangle|^2 \right)^{1/2} , \tag{3}$$

with $\langle q_{6m}(i) \rangle = 1/(N_n(i)+1) \sum_{j=0}^{N_n(i)} q_{6m}(j)$, where the sum is over particle i and all the N_n neighbor molecules. We note that q_{6m} is the order parameter defined in Eq. (1) with an l value of 6.

As shown in Fig. 3(a), although q_{n6} does not readily distinguish the two forms of ice, it does clearly separate ice from water, with the liquid having q_{n6} below 0.35. Thus, we first utilize the q_{n6} parameter to distinguish ice and liquid. Then for ice, $c(i,j)$ is used to distinguish between Ih and Ic. The final protocol for water molecule classification is summarized in Fig. 4.

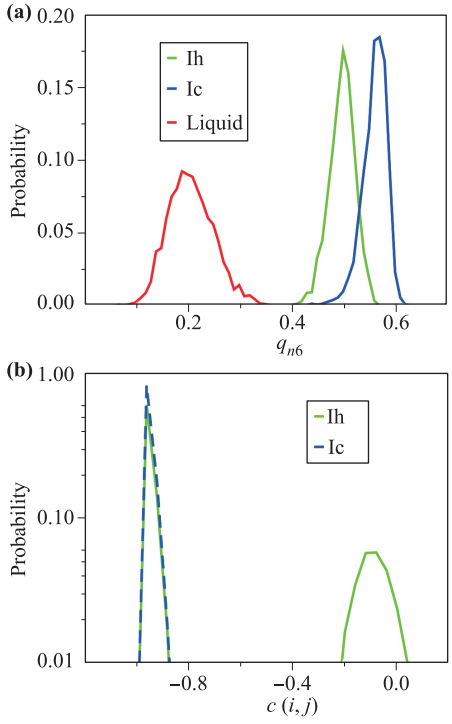

Fig. 3 Orientational order parameters for forms of liquid water, ice Ic and ice Ih. **(a)** The probability of the neighbor average orientational order parameter q_{n6} for bulk ice Ih, ice Ic and liquid water. **(b)** The probability of the correlation of orientational order parameter $c(i, j)$ for ice Ih and ice Ic.

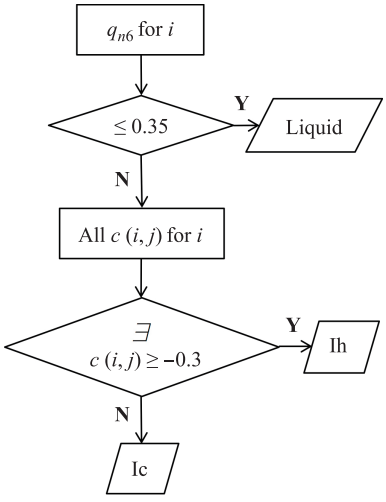

Fig. 4 Flow diagram for water molecule classification.

2.3 Identifying the growth interface

The growth rate is measured by the motion of the growth interface, which can be identified with the z-density profile of oxygen. The z-density profile is produced with a bin width of 0.5 Å. Figure 5 shows a snapshot of such an oxygen z-density profile. As mentioned previously, the z direction is normal to the (0001) plane of ice Ih (basal plane), which is also the (111) plane of ice Ic. As shown in Fig. 5, the z-density in the ice region is composed of double peaks separated by regions of zero density. Owing to the tetrahedral orientation of the hydrogen bonds, water in the basal plane is buckled, giving rise to the double peaks. We refer to each double peak as a bilayer of water. Each water molecule forms three hydrogen bonds with other water molecules inside the bilayer. To satisfy the ice rules, each water molecule has to form a fourth hydrogen bond with a water molecule in a different bilayer. Owing to the angular constraint, the orientation of this last hydrogen bond is approximately normal to the basal plane, leading to a region of zero density approximately 0.2 nm wide. As ice growth is primarily bilayer-by-bilayer (vide infra), we define the growth surface to be approximately 0.1 nm above the last stable bilayer for the calculation of the growth rate.

3 Results and discussion

3.1 Growth mechanism based on prefreezing layer

Figure 6 shows the location of the growth interface as a function of time at 240 K. The growth behaviors at other temperatures are similar. A key observation from the location of the growth interface is the fluctuations between two bilayers that occur much more frequently than the advance of the ice interface to form a third bi-

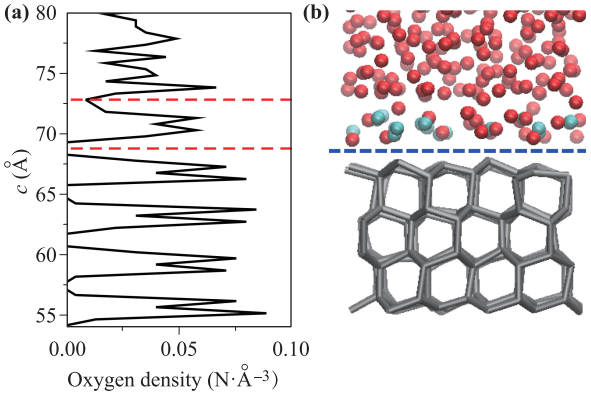

Fig. 5 Identification of growth interface and the pre-freezing layer. **(a)** The oxygen z-density profile. The red dashed line at the bottom is the growth interface. The region between two red dashed lines is the location of pre-freezing layer. **(b)** The snapshot from the simulation of (a). Hydrogen bonds in ice layers are grey lines, in liquid region, red spheres are molecules which have q_{n6} below 0.35, and cyan spheres are molecules which have q_{n6} over 0.35, that is, ice-like. All the water molecules in the pre-freezing layers are cyan. The blue dashed line is the growth interface.

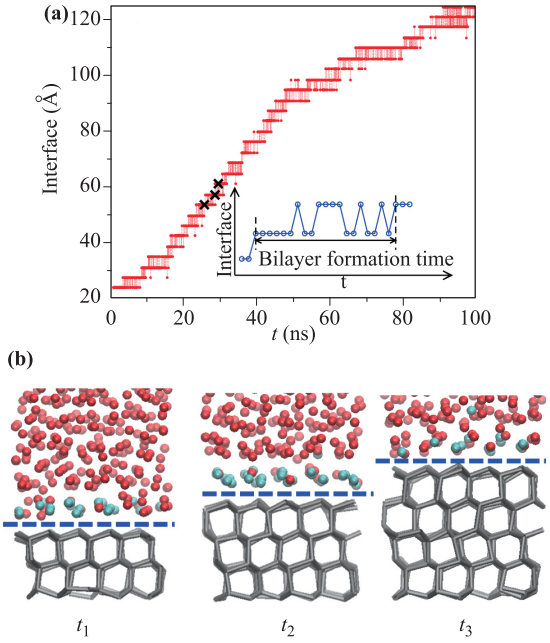

Fig. 6 The process of ice growth and the bilayer formation time. **(a)** The location of interface as a function of time at $T = 240$ K. The snapshots of time at the three stars are shown in **(b)**. $t_1 = 25\,830$ ps, $t_2 = 28\,730$ ps and $t_3 = 29\,650$ ps.

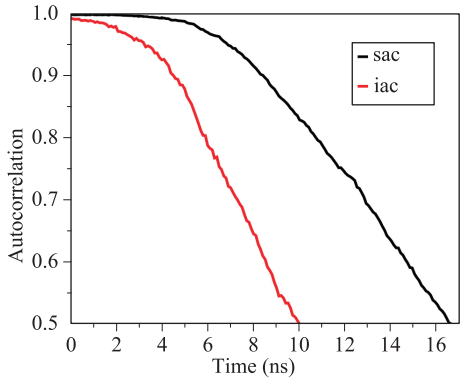

Fig. 7 The state and identity autocorrelation functions for the growth interface at $T = 240$ K. When 85% water molecules are ice-like, only 50% of them have the same identity as the final formation.

layer. In Fig. 6, the formation time of a bilayer is marked. A bilayer is considered to be formed when fluctuations with its sub-bilayer no longer occur. After the bilayer is formed, the identity of the ice molecules in this bilayer no longer changes except in rare cases, when structural defects in the formed ice are then healed.

Figure 7 shows the state autocorrelation function (*sac*) and the identity autocorrelation function (*iac*) for the growth interface. With the water identity function,

$$id(i) = \begin{cases} 0, & i \in \text{liquid} \\ 1, & i \in \text{ice Ih} \\ 2, & i \in \text{ice Ic} \end{cases}, \tag{4}$$

where each water i is classified based on the procedure described in Section 2.2, the identity autocorrelation function is calculated as

$$iac(t) = \frac{1}{N}\sum \delta_{(id(i(0)))id(i(-t))}\ , \tag{5}$$

where the sum is over the N water molecules in the bilayer of interest, the Kronecker δ function is one when the identity of water at time t before time zero is the same as that at time zero. Time zero is the time of formation for this bilayer of ice. The state correlation function is

$$sac(t) = \frac{1}{N}\sum H\left[id(i(0))\cdot id(i(-t)) - \frac{1}{2}\right]\ , \tag{6}$$

where the sum is over the N water molecules in the bilayer of interest, and H is the Heaviside step function. It is worth emphasizing that both the *sac* and *iac* at time t indicate the correlation at time t before the formation of ice, whereas the contribution to the *iac* goes to zero as soon as the water changes its identity, the contribution to *sac* goes to zero only if the water becomes liquid.

It is clear from Fig. 7 that 10 ns before the formation of ice, half of the water does not have the same identity as the final formed ice. However, the number of liquid molecules is only 15% at approximately 10 ns before the formation. A close inspection of the trajectories indicates that the water molecules on top of the last bilayer of ice quickly gain order, as a result of the templating effect of the top ice layer. After the top bilayer of ice is formed, each water molecule will project a hydrogen bond normal to the ice surface. Guided by the hydrogen bond, liquid water quickly aligns itself, losing translational motion thus becoming ice-like. We refer to this layer on top of the formed ice as the prefreezing layer. Because each water forms three hydrogen bonds with other molecules within each bilayer, guided by the ice sublayer, the water molecules in the prefreezing layer quickly form three hydrogen bonds among each other, and thus the gain in enthalpy from hydrogen bond formation compensates for the loss of entropy of translational motion, leading to rapid growth of ice below T_M.

Whereas the water in the prefreezing layer quickly becomes ice, as indicated by the large q_{n6} value of 0.35 or higher as discussed previously, the fast local structural relaxation leads to a mixture of ice Ic and ice Ih molecules in the prefreezing layer. The different lattice positions of ice Ih and ice Ic lead to a kinetic barrier for the advancement of the growth interface. Thus, the final formation of a crystalline ice bilayer is an activated process involving the local competition of Ih and Ic molecules and is a slow

step of the growth kinetics. In our work, the ice growth rate is approximately 4.4 ns (vide infra); from Fig. 7, the number of ice molecules in the prefreezing layer increases to 95% at 6.8 ns before the formation of the ice bilayer. This supports the relaxation of ice-like water particles into a uniform crystalline surface being rate-limiting at the growth temperature. We note that this prefreezing-layer-based growth mechanism is more complex than a standard two-dimensional nucleation and growth mechanism frequently expected for epitaxial growth. If water in the prefreezing layer can be considered as a metastable disordered ice in two dimensions, the growth mechanism would thus be consistent with the prediction of the Oswald ripening rules, which state that the least stable polymorph would crystallize before the most stable one. In this case, the two-dimensional disordered ice is the less stable polymorph.

We anticipate similar prefreezing layers composed of ice-like water with significantly reduced translational motion to occur at other flat and hydrophobic interfaces. A flat surface reduces the entropy of translational motion normal to the interface. This reduction in entropy will reduce the free energy barrier for the formation of ice. The formation of a prefreezing layer due to the templating effect of ice surfaces explains the relatively fast growth kinetics of ice when compared to nucleation. Although water can be easily supercooled, it is known experimentally to be a poor glass former [49, 50]. Below the homogenous nucleation temperature, ice crystal grows fast, posing challenges for the liquid to enter into a glassy state by cooling. This is consistent with the templating effects of ice surfaces, leading to fast growth of additional layers through the prefreezing layer. Without microscopic crystals to partially pre-ordered liquid, the formation of the initial nuclei is kinetically challenging, consistent with the observed stability of ice over extended periods of time under mildly supercooled conditions.

3.2 Growth rate and growth retardation

The formation time (also growth time) of each bilayer of ice is measured as the time between when the ice sublayer is fully formed and when the prefreezing layer is fully converted to ice. Figure 8 shows the average growth rate as a function of temperature. The rate of growth is not monotonic, showing a maximum at 250 K, which is approximately 20 K of supercooling. The existence of a maximum in the growth rate is not surprising considering the increase in the driving force for ice formation as the free energy difference increases and the slower kinetics at lower temperatures. It is worth emphasizing that the maximum growth rate revealed by the simulations is for ice growth on an existing basal surface. It does not provide information regarding nucleation rates. However, for the growth of existing ice, our simulation indicates

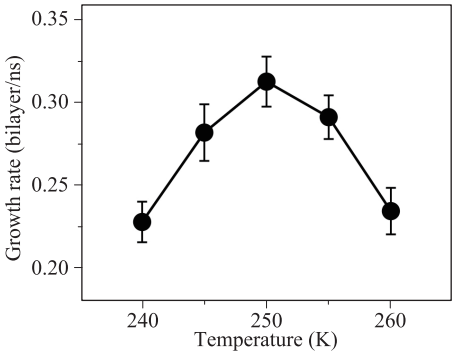

Fig. 8 The growth rates changes nonlinearly with temperature, with the maximum at 250 K.

an optimal supercooling of 20 K for the fastest crystal growth. This would also be the optimal growth temperature under conditions where fast heterogeneous nucleation is present. This temperature is consistent with the experimental observation that ice growth rate increases at up to 18 K of supercooling.

Figure 9 shows a distribution of the growth time of each bilayer at each temperature. It can be seen that the growth time distribution has a long tail, especially for temperatures above and below the 250 K maximum rate temperature. In order to better understand the slow events, all bilayer growth events with a growth time longer than 16 ns were carefully studied. There are a total of 79 such events across the five growth temperatures (Table 1). It is interesting that different mechanisms are responsible for the slow bilayer growth events at higher and lower temperatures.

At higher temperatures, such as 260 K, it can be seen for several growth events that *sac* oscillates, as shown in Fig. 10. This indicates that the state order in the prefreezing layer first increases and then decreases. During the growth of a typical bilayer, the order in the prefreezing layer increases gradually until most surface water is disordered ice, and the kinetic slow step is the rearrangement of disordered ice into crystalline ice. At a temperature close to T_M, the relative free energy difference be-

Table 1 Classification of slow bilayer growth events at each temperature. A slow bilayer growth event is defined when the next bilayer takes longer than 16 ns to grow.

Temperature	Total	Remelting	Defect
240 K	28	0	8
245 K	12	4	8
250 K	4	2	2
255 K	5	4	1
260 K	30	30	0

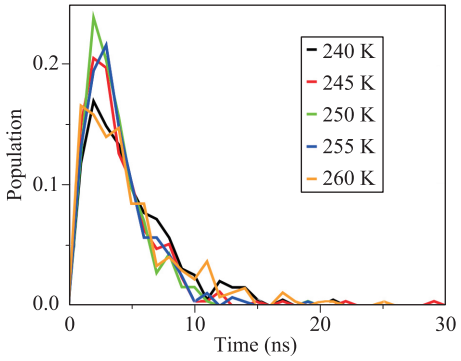

Fig. 9 The distribution of the bilayer growth time. At $T =$ 245–255 K, most cases have growth time within 10 ns, while at 240 K and 260 K, some more cases have growth time longer than 16 ns.

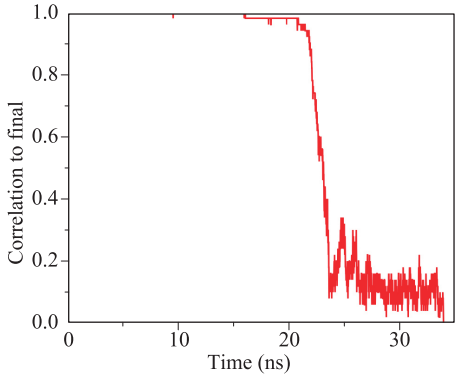

Fig. 10 The state autocorrelation function of one case at $T = 260$ K. During 25–23 ns before the bilayer growth finish, water molecules crystalized then melted again.

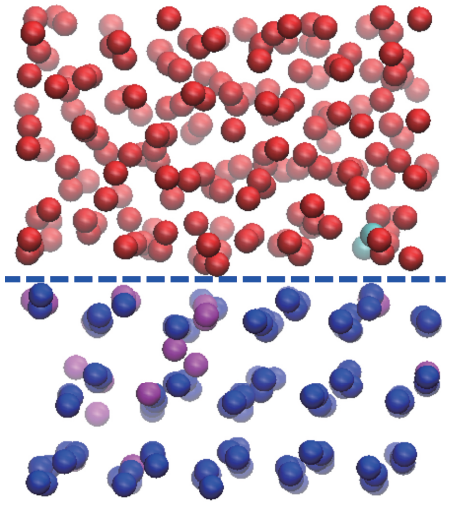

Fig. 11 Water molecules are trapped in the ice layers. A snapshot from the simulation at $T = 240$ K. Blue spheres are ice Ic molecules in the ice layers. Magenta spheres are water molecules trapped in the ice layers, that are, defects.

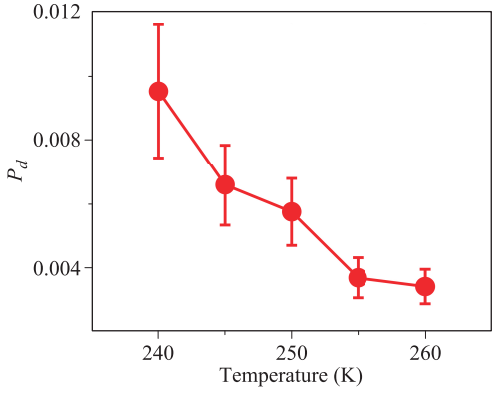

Fig. 12 The degree of defect changes with temperature. There are more long-lifetime defects at lower temperature.

tween ice and water is small, the balance of entropic loss and the enthalpy gain is subtler, and thus the prefreezing layer can have its state order reduced, which leads to delays in the buildup of disordered ice slowing down the first stage of ice growth. We refer to this mechanism as remelting-induced growth retardation, which involves oscillations of the number of disordered ice molecules in the prefreezing layer.

The origin for the slow bilayer growth at lower temperatures is even more intriguing. During growth, water molecules may be trapped in defect positions in the prefreezing layer, thereby preventing the prefreezing layer from reaching "prefect" order for ice bilayers. Such trapping leads to defect-induced retardation of ice growth. As the growth interface advances, defects could then be buried in the ice layers. Figure 11 shows a configuration in which water molecules are trapped in the top ice layer. Such water molecules do not reside in the correct lattice positions for ice and are classified as "liquid" according to the q_{n6}-based criterion used in this work. Whereas each defect should eventually heal, the lifetime of the defects grows as the temperature decreases. From Fig. 11, we can see that the trapped defects prevent all the water molecules in the prefreezing layer from settling into the proper lattice position. The formation of the next ice layer on top of the defect will be slowed down, which also contributes to defect-induced growth retardation.

We note that our study reveals two types of defect-induced retardation, which are closely related. In one case, defects in the prefreezing layer are slow to heal, leading to retardation of the advance of the growth interface. Thus, the lower temperature slows down the activated conversion of disordered ice into ordered ice. For the other mechanism, defects in the top ice layer prevent the growth of the next prefreezing layer. Most defects in the prefreezing layer eventually heal, whereas some de-

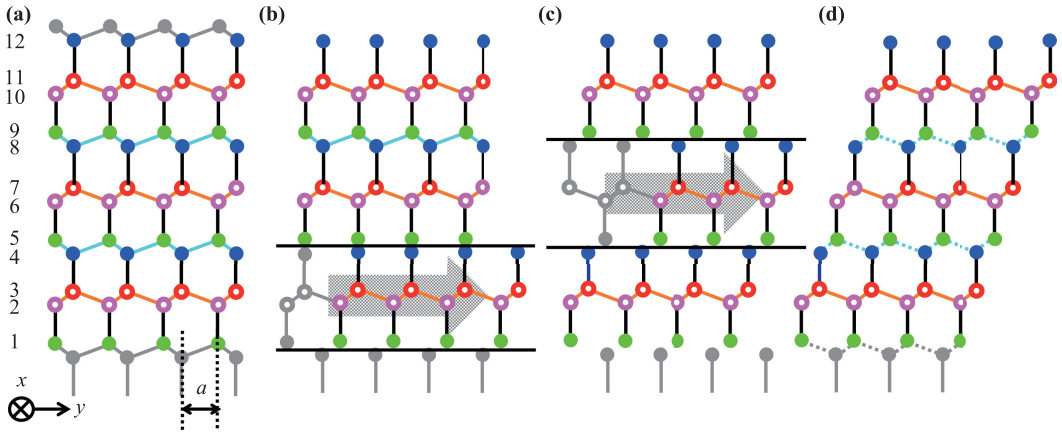

Fig. 13 The transformation of ice Ic and ice Ih. **(a)** 12 monolayers stack in an ABAB pattern in ice Ih. **(b)** Monolayers 1 to 4 are translated by a in y direction. **(c)** Monolayers 7 to 8 are translated by $2a$ in y direction. **(d)** 12 monolayers stack in an ABCABC pattern in ice Ic. The grey ones are oxygens and hydrogen bonds in other periods. Dotted bonds are new bonds created after transition. a is the distance of two bonded oxygens in x–y projection.

fects do get buried into ice. Figure 12 reports the degree of defects buried in the ice layers. At lower temperatures, a higher defect rate can be observed, which is consistent with slower kinetics for defect healing when supercooling is stronger.

3.3 Transformation between ice Ic and ice Ih

It is worth mentioning that both ice Ih and ice Ic grow with similar probability, regardless of sublayer structures. The freshly grown ice is thus stacking-disordered. Ice Ic does not convert spontaneously to ice Ih in the vast majority of cases in the time and space scale of our simulation. In cases where the transition occurs, the Ic phase melts and the Ih phase forms afterwards. As is clear from Fig. 13, a solid-state transition from one form of ice to another requires two ice bilayers to rearrange. The transformation of ice Ih to ice Ic would require a two-step translation of monolayers in the x–y plane: in every 12 monolayers, first translate one to four monolayers by $a/\sqrt{3}$ in the y direction; and then translate five to eight monolayers by $2a/\sqrt{3}$ in the y direction. a is the length of the ice Ih lattice in the y direction. Such motion, which requires extensive reorganization of hydrogen bonds, is likely to be associated with a large activation barrier in a crystalline state. Partial remelting of ice thus is likely to be one of the major pathways for the relaxation of ice Ic into ice Ih, even for microscopic systems. Experimentally, ice Ic has been observed to have a long lifetime at or below 240 K [51, 52]. The lowest temperature at which remelting is observed in our simulation is approximately 245 K. We assume 245 K is indeed close to the minimum temperature at which transient remelting through structural fluctuation is significant. This would explain the difficulty in obtaining ice Ic experimentally above 240 K.

4 Conclusion

Starting from 20 initial conformations with different proton arrangements, the growth of ice was studied at five different temperatures from 240 to 260 K using the WAIL model, which has a melting temperature of approximately 270 K. As the temperature decreases, the growth rate of ice initially increases and then decreases, with a maximum rate observed at approximately 20 K below the freezing temperature. This estimate is consistent with existing experimental evidence, which shows a monotonic increase of the growth rate at up to 18 K supercooling.

It was found that ice growth is predominately bilayer-by-bilayer. Water on top of the growth surface losses translational motion normal to the interface, and at the same time the templating effects of the ice surface facilitate the formation of a prefreezing layer. The water in the prefreezing layer freezes in a two-step process. In the first step, water quickly forms disordered ice above the growth interface. This is followed by a slow conversion from disordered ice into ordered ice, which is the rate-limiting step for ice growth. At a relatively low degree of supercooling, re-melting of the prefreezing layer occurs frequently and leads to slow growth events. At lower temperatures, defects formed in the prefreezing layer impede ice growth and also lead to slower growth events. Our study shows the newly grown ice is stacking-disordered with the ice Ic growth rate slightly higher than that of ice Ih below 260 K. It is hypothesized that the re-melting of the ice–liquid interface due to structural fluctuations plays an important role in the transformation of ice Ic into ice Ih.

Our study improves the understanding of the crystallization of ice on surfaces. The molecular dynamics observation of stacking and rearrangements during growth is a powerful tool to establish the molecular mechanisms of crystal growth. The same analysis by visualizing molecular dynamics in the interface can be applied to investigate other crystals and provide useful insights into the growth process.

Acknowledgements This work was supported by the National Basic Research Program of China under Grant No. 2015CB856801, the National Natural Science Foundation of China under Grant Nos. 11525520 and 11290162/A040106, and the National Key R&D Program under Grant No. 2016YFA0300901. The computer resources for this study were provided by the Arkansas High Performance Computational Center through grant MRI-R2 0959124 provided by the NSF of USA.

References

1. V. De Michele, G. Romanelli, and A. Cupane, Dynamics of supercooled confined water measured by deep inelastic neutron scattering, *Front. Phys.* 13(1), 138205 (2018)
2. M. De Marzio, G. Camisasca, M. Rovere, and P. Gallo, Fragile to strong crossover and Widom line in supercooled water: A comparative study, *Front. Phys.* 13(1), 136103 (2018)
3. E. O. Rizzatti, M. A. A. Barbosa, and M. C. Barbosa, Core-softened potentials, multiple liquid–liquid critical points, and density anomaly regions: An exact solution, *Front. Phys.* 13(1), 136102 (2018)
4. F. Mallamace, C. Corsaro, D. Mallamace, Z. Wang, and S. H. Chen, The Boson peak in confined water: An experimental investigation of the liquid-liquid phase transition hypothesis, *Front. Phys.* 10(5), 106103 (2015)
5. F. Mallamace, C. Corsaro, D. Mallamace, N. Cicero, S. Vasi, G. Dugo, and H. E. Stanley, Dynamical changes in hydration water accompanying lysozyme thermal denaturation, *Front. Phys.* 10(5), 106104 (2015)
6. F. Mallamace, C. Corsaro, D. Mallamace, C. Vasi, N. Cicero, and H. E. Stanley, Water and lysozyme: Some results from the bending and stretching vibrational modes, *Front. Phys.* 10(5), 106105 (2015)
7. I. Piazza, A. Cupane, E. L. Barbier, C. Rome, N. Collomb, J. Ollivier, M. A. Gonzalez, and F. Natali, Dynamical properties of water in living cells, *Front. Phys.* 13(1), 138301 (2018)
8. D. Mallamace, S. Vasi, M. Missori, F. Mallamace, and C. Corsaro, NMR investigation of degradation processes of ancient and modern paper at different hydration levels, *Front. Phys.* 13(1), 138202 (2018)
9. F. Martelli, H. Y. Ko, C. C. Borallo, and G. Franzese, Structural properties of water confined by phospholipid membranes, *Front. Phys.* 13(1), 136801 (2018)
10. C. Corsaro, F. Mallamace, S. Vasi, S. H. Chen, H. E. Stanley, and D. Mallamace, Contrasting microscopic interactions determine the properties of water/methanol solutions, *Front. Phys.* 13(1), 138201 (2018)
11. A. Parmentier, C. Andreani, G. Romanelli, J. J. Shephard, C. G. Salzmann, and R. Senesi, Hydrogen mean force and anharmonicity in polycrystalline and amorphous ice, *Front. Phys.* 13(1), 136101 (2018)
12. H. Shen, M. Chen, Z. Sun, L. Xu, E. Wang, and X. Wu, Signature of the hydrogen-bonded environment of liquid water in X-ray emission spectra from first-principles calculations, *Front. Phys.* 13(1), 138204 (2018)
13. A. Gabrieli, M. Sant, S. Izadi, P. S. Shabane, A. V. Onufriev, and G. B. Suffritti, High-temperature dynamic behavior in bulk liquid water: A molecular dynamics simulation study using the OPC and TIP4P-Ew potentials, *Front. Phys.* 13(1), 138203 (2018)
14. T. Bartels-Rausch, Ten things we need to know about ice and snow, *Nature* 494(7435), 27 (2013)
15. J. Liang, M. Liu, R. Wang, and Y. Wang, Study on the glaze ice accretion of wind turbine with various chord lengths, *IOP Conf. Ser.: Earth Environ. Sci.* 121, 042026 (2018)
16. S. Zhang, J. Huang, Y. Cheng, H. Yang, Z. Chen, and Y. Lai, Bioinspired surfaces with superwettability for anti-icing and ice-phobic application: Concept, mechanism, and design, *Small* 13(48), 1701867 (2017)
17. J. D. Atkinson, B. J. Murray, M. T. Woodhouse, T. F. Whale, K. J. Baustian, K. S. Carslaw, S. Dobbie, D. O'Sullivan, and T. L. Malkin, The importance of feldspar for ice nucleation by mineral dust in mixed-phase clouds, *Nature* 498(7454), 355 (2013)
18. Y. Jin, Z. He, Q. Guo, and J. Wang, Control of ice propagation by using polyelectrolyte multilayer coatings, *Angew. Chem. Int. Ed. Engl.* 56(38), 11436 (2017)
19. I. K. Voets, From ice-binding proteins to bio-inspired antifreeze materials, *Soft Matter* 13(28), 4808 (2017)
20. Y. Xu, N. G. Petrik, R. S. Smith, B. D. Kay, and G. A. Kimmel, Homogeneous nucleation of ice in transiently-heated, supercooled liquid water films, *J. Phys. Chem. Lett.* 8(23), 5736 (2017)
21. C. A. Knight, A simple technique for growing large, optically "perfect" ice crystals, *J. Glaciol.* 42(142), 585 (1996)
22. A. Shibkov, Y. I. Golovin, M. Zheltov, A. Korolev, and A. Leonov, In situ monitoring of growth of ice from supercooled water by a new electromagnetic method, *J. Cryst. Growth* 236(1–3), 434 (2002)
23. Y. Qiu, N. Odendahl, A. Hudait, R. Mason, A. K. Bertram, F. Paesani, P. J. DeMott, and V. Molinero, Ice nucleation efficiency of hydroxylated organic surfaces is controlled by their structural fluctuations and mismatch to ice, *J. Am. Chem. Soc.* 139(8), 3052 (2017)

24. M. Matsumoto, S. Saito, and I. Ohmine, Molecular dynamics simulation of the ice nucleation and growth process leading to water freezing, *Nature* 416(6879), 409 (2002)
25. D. Rozmanov and P. G. Kusalik, Temperature dependence of crystal growth of hexagonal ice (Ih), *Phys. Chem. Chem. Phys.* 13(34), 15501 (2011)
26. H. Pruppacher, On the growth of ice crystals in supercooled water and aqueous solution drops, *Pure and Applied Geophysics* 68(1), 186 (1967)
27. J. Hallett, Experimental studies of the crystallization of supercooled water, *J. Atmos. Sci.* 21(6), 671 (1964)
28. N. Fukuta, Experimental studies on the growth of small ice crystals, *J. Atmos. Sci.* 26(3), 522 (1969)
29. D. Rozmanov and P. G. Kusalik, Anisotropy in the crystal growth of hexagonal ice Ih, *J. Chem. Phys.* 137(9), 094702 (2012)
30. A. A. Shibkov, M. A. Zheltov, A. A. Korolev, A. A. Kazakov, and A. A. Leonov, Crossover from diffusion-limited to kinetics-limited growth of ice crystals, *J. Cryst. Growth* 285(1–2), 215 (2005)
31. M. S. Razul and P. G. Kusalik, Crystal growth investigations of icewater interfaces from molecular dynamics simulations: Profile functions and average properties, *J. Chem. Phys.* 134(1), 014710 (2011)
32. E. R. Pinnick, S. Erramilli, and F. Wang, Predicting the melting temperature of ice-Ih with only electronic structure information as input, *J. Chem. Phys.* 137(1), 014510 (2012)
33. M. Fitzner, G. C. Sosso, S. J. Cox, and A. Michaelides, The many faces of heterogeneous ice nucleation: Interplay between surface morphology and hydrophobicity, *J. Am. Chem. Soc.* 137(42), 13658 (2015)
34. E. Sanz, C. Vega, J. R. Espinosa, R. Caballero-Bernal, J. L. Abascal, and C. Valeriani, Homogeneous ice nucleation at moderate supercooling from molecular simulation, *J. Am. Chem. Soc.* 135(40), 15008 (2013)
35. J. R. Espinosa, E. Sanz, C. Valeriani, and C. Vega, Homogeneous ice nucleation evaluated for several water models, *J. Chem. Phys.* 141(18), 18C529 (2014)
36. A. Haji-Akbari and P. G. Debenedetti, Direct calculation of ice homogeneous nucleation rate for a molecular model of water, *Proc. Natl. Acad. Sci. USA* 112(34), 10582 (2015)
37. G. E. Lindberg and F. Wang, Efficient sampling of ice structures by electrostatic switching, *J. Phys. Chem. B* 112(20), 6436 (2008)
38. D. Van Der Spoel, E. Lindahl, B. Hess, G. Groenhof, A. E. Mark, and H. J. Berendsen, GROMACS: Fast, flexible, and free, *J. Comput. Chem.* 26(16), 1701 (2005)
39. T. L. Malkin, B. J. Murray, A. V. Brukhno, J. Anwar, and C. G. Salzmann, Structure of ice crystallized from supercooled water, *Proc. Natl. Acad. Sci. USA* 109(4), 1041 (2012)
40. K. Morishige and H. Uematsu, The proper structure of cubic ice confined in mesopores, *J. Chem. Phys.* 122(4), 044711 (2005)
41. J. Benet, L. G. MacDowell, and E. Sanz, A study of the ice-water interface using the TIP4P/2005 water model, *Phys. Chem. Chem. Phys.* 16(40), 22159 (2014)
42. T. L. Malkin, B. J. Murray, C. G. Salzmann, V. Molinero, S. J. Pickering, and T. F. Whale, Stacking disorder in ice I, *Phys. Chem. Chem. Phys.* 17(1), 60 (2015)
43. L. Scott, A primer on ice (in preparation) (2012)
44. S. Choi, E. Jang, and J. S. Kim, In-layer stacking competition during ice growth, *J. Chem. Phys.* 140(1), 014701 (2014)
45. P. Rein ten Wolde, M. J. Ruiz-Montero, and D. Frenkel, Numerical calculation of the rate of crystal nucleation in a Lennard-Jones system at moderate undercooling, *J. Chem. Phys.* 104(24), 9932 (1996)
46. E. B. Moore, E. de la Llave, K. Welke, D. A. Scherlis, and V. Molinero, Freezing, melting and structure of ice in a hydrophilic nanopore, *Phys. Chem. Chem. Phys.* 12(16), 4124 (2010)
47. A. H. Nguyen and V. Molinero, Identification of clathrate hydrates, hexagonal ice, cubic ice, and liquid water in simulations: The CHILL+ algorithm, *J. Phys. Chem. B* 119(29), 9369 (2015)
48. A. Reinhardt, J. P. Doye, E. G. Noya, and C. Vega, Local order parameters for use in driving homogeneous ice nucleation with all-atom models of water, *J. Chem. Phys.* 137(19), 194504 (2012)
49. H. Tanaka, Simple view of waterlike anomalies of atomic liquids with directional bonding, *Phys. Rev. B* 66(6), 064202 (2002)
50. C. A. Angell, R. D. Bressel, M. Hemmati, E. J. Sare, and J. C. Tucker, Water and its anomalies in perspective: Tetrahedral liquids with and without liquid–liquid phase transitions, *Phys. Chem. Chem. Phys.* 2(8), 1559 (2000)
51. T. C. Hansen, M. M. Koza, P. Lindner, and W. F. Kuhs, Formation and annealing of cubic ice (II): Kinetic study, *J. Phys.: Condens. Matter* 20(28), 285105 (2008)
52. W. F. Kuhs, C. Sippel, A. Falenty, and T. C. Hansen, Extent and relevance of stacking disorder in "ice I(c)", *Proc. Natl. Acad. Sci. USA* 109(52), 21259 (2012)